AD-A049 343 NORTH CAROLINA STATE UNIV RALEIGH DEPT OF MECHANICAL--ETC F/G 20/4
LIFT HYSTERESIS OF AN OSCILLATING SLENDER ELLIPSE.(U)
SEP 77 W D JOHNSON, J C WILLIAMS DAHC04-75-G-0007
ARO-10157.7-E NL

UNCLASSIFIED

1 OF

AD A049343

END
DATE FILMED
3-78
DDC

(18) ARO (19) 10157.7-E

(6)

LIFT HYSTERESIS OF AN OSCILLATING SLENDER ELLIPSE

(12)

(9) Interim Technical Report

(12) 145 p.

(10) W. Donald Johnson and J. C. Williams III

(11) 30 September 30, 1977

U. S. Army Research Office
Grant No. DAHCO4-75-G-0007

(15) DA-ARO-D-31-124-72-G134

Department of Mechanical and Aerospace Engineering
School of Engineering
North Carolina State University
Raleigh, North Carolina

400 714

THE FINDINGS IN THIS REPORT ARE NOT TO BE CONSTRUED AS AN OFFICIAL DEPARTMENT OF THE ARMY POSITION, UNLESS SO DESIGNATED BY OTHER AUTHORIZED DOCUMENTS.

Security Classification

DOCUMENT CONTROL DATA - R & D

(Security classification of title, body of abstract and indexing annotation must be entered when the overall report is classified)

1. ORIGINATING ACTIVITY (Corporate author)	2a. REPORT SECURITY CLASSIFICATION
Department of Mechanical and Aerospace Engineering North Carolina State University Raleigh, North Carolina 27607	Unclassified
	2b. GROUP NA

3. REPORT TITLE

LIFT HYSTERESIS OF AN OSCILLATING SLENDER ELLIPSE

4. DESCRIPTIVE NOTES *(Type of report and inclusive dates)*

Interim Technical Report

5. AUTHOR(S) *(First name, middle initial, last name)*

Walter D. Johnson and James C. Williams, III

6. REPORT DATE	7a. TOTAL NO. OF PAGES	7b. NO. OF REFS
September 30, 1977	37	15

8a. CONTRACT OR GRANT NO.	9a. ORIGINATOR'S REPORT NUMBER(S)
DAH C04-75-G007 and b. PROJECT NO. DA-ARO-D-31-124-72-G134	NA
c.	9b. OTHER REPORT NO(S) *(Any other numbers that may be assigned this report)*
d.	NA

10. DISTRIBUTION STATEMENT

Approved for public release; distribution unlimited

11. SUPPLEMENTARY NOTES	12. SPONSORING MILITARY ACTIVITY
NA	U.S. Army Research Office Post Office Box 12211 Research Triangle Park, N. C. 27709

13. ABSTRACT

A theoretical investigation has been made to determine the variation of lift with time on a slender elliptic cylinder oscillating in pitch. The development of the unsteady two-dimensional laminar boundary layer over the surfaces of the pitching ellipse is calculated and the periodic variation of lift is determined by matching the rate at which boundary layer developed vorticity is shed into the wake with the time rate of change of circulation about the ellipse. The effects of mean angle-of-attack and oscillation frequencies on lift hysteresis loops are determined. It is shown that the hysteresis loops change direction for mean angles of attack greater than that corresponding to maximum steady state lift.

DD FORM 1 NOV 68 1473 REPLACES DD FORM 1473, 1 JAN 64, WHICH IS OBSOLETE FOR ARMY USE.

Unclassified

Security Classification

14. KEY WORDS	LINK A		LINK B		LINK C	
	ROLE	WT	ROLE	WT	ROLE	WT
Lift Hysteresis						
Dynamic Stall						

LIFT HYSTERESIS OF AN OSCILLATING SLENDER ELLIPSE

by

W. Donald Johnson

and

James C. Williams, III

TABLE OF CONTENTS

LIST OF FIGURES

LIST OF TABLES

LIFT HYSTERESIS OF AN OSCILLATING SLENDER ELLIPSE

ABSTRACT

A theoretical investigation has been made to determine the variation of lift with time on a slender elliptic cylinder oscillating in pitch. The development of the unsteady two-dimensional laminar boundary layer over the surfaces of the pitching ellipse is calculated and the periodic variation of lift is determined by matching the rate at which boundary layer developed vorticity is shed into the wake with the time rate of change of circulation about the ellipse. The effects of mean angle-of-attack and oscillation frequencies on lift hysteresis loops are determined. It is shown that the hysteresis loops change direction for mean angles of attack greater than that corresponding to maximum steady state lift.

INTRODUCTION

In recent years, several practical problems encountered in the design of helicopter rotors and axial compressors have spurred interest in the effect of unsteady stall on the lift of blades undergoing periodic changes in angle-of-attack. The variation of lift with angle-of-attack for unsteady flow is vastly different in the stall region from the familiar static lift curve. In the steady case there is a sharp decrease in lift at angles-of-attack greater than the stall angle, whereas in the unsteady oscillatory case tests by Halfman et al[1] indicate that the maximum dynamic lift coefficient is greater than the static $C_{\ell_{max}}$. Liiva et al[2] experimentally obtained hysteresis loops in the vicinity of the steady stall angle of attack on two-dimensional airfoils sinusoidally oscillating about a mean angle-of

attack. This study indicates that lift hysteresis is strongly influenced by frequency, oscillation amplitude, and mean angle-of-attack.

Several investigations have been performed which are inviscid in basic formulation but include empirical estimates of the viscous effects. Ham[3] developed a theory for two-dimensional dynamic stall by modeling the process with discrete vortices shed from the leading edge. Ericsson and Reding[4] developed a quasi-steady analytical method in which airfoil static aerodynamic data may be used to predict the unsteady variations in lift and moment. While methods such as these may be useful in making predictions of unsteady aerodynamic effects, they do not go to the root of the problem. Basically, stall is a phenomenon which is directly related to boundary layer separation and any complete analysis of stall, either steady or unsteady, must include the effect of boundary layer separation.

Several investigators have modeled unsteady stall including the effects of boundary layer development. Crimi[5] analyzed the flow about an airfoil undergoing unsteady motion by modeling the basic flow elements and considering interactions between the inviscid and viscous flows by iterative techniques. His work seems limited by a linearized description of the potential flow which is solved numerically for each time step by considering a distribution of source and sink singularities. Patay[6] used a boundary layer analysis to study the effect of leading edge separation on the delay of dynamic stall for pitching Joukowski airfoils. This study employs a momentum integral procedure but solves only a quasi-steady description of the flow process. Moore[7] considered the problem of predicting the lift on a slender elliptic cylinder in a free stream oscillating in angle-of-attack. In addition to considering a stationary cylinder in an oscillating stream, Moore simplified his analysis by limiting the problem to the case of maximum static lift and by considering

only small rates of change of incidence. By restricting his analysis to maximum steady state lift, Moore eliminates the quasi-steady variation in circulation. In the lift versus angle-of-attack curve, Moore obtains a hysteresis loop whose direction is counterclockwise, in contrast to the clockwise direction of hysteresis loops obtained experimentally on cylinders of airfoil cross-section. Sears[8] reviewed Moore's work and suggested that further investigations of this type be made. Sears discussed the effects of Moore's assumptions and stated that "... the dominant effect in this hysteresis may arise from quasi-steady terms that Moore eliminated by considering small perturbations from maximum lift."

The present study, which is not restricted to maximum steady state lift and includes the quasi-steady variations in circulation, examines the unsteady viscous flow about a 6:1 elliptic cylinder oscillating periodically in a stationary uniform stream. The major reason for choosing this type body is that the inviscid flow about an elliptic cylinder is analytic and easily expressed in closed form. The analysis includes representation of the unsteady velocity components as a steady-state term plus the first term of a power series expansion as well as transformation of the coordinate system such that the separation point appears steady in the transformed coordinate. The differential equations resulting from the boundary layer formulation were solved using an unsteady momentum integral technique. The unsteady circulation as a function of the periodically varying angle-of-attack was determined by iteration using the revised Taylor-Howarth criterion for relating the rate at which boundary layer developed vorticity is shed into the wake to the time rate of change of circulation.

The results, which are presented for a range of mean incidence angles and oscillation frequencies, describe the behavior of the unsteady boundary

layer and illustrate dynamic stall, including lift hysteresis.

ANALYSIS

The coordinate system and body orientation used in the present study is presented in Figure 1. The x coordinate, which is measured from the stagnation point for steady flow at the mean angle-of-attack, is positive on the upper surface and negative on the lower surface. The angle η is measured positive counterclockwise from the trailing edge in a body fixed system. The angle-of-attack, $\alpha(t)$, is assumed positive when the leading edge is pitched up relative to the direction of the stream.

Potential Flow

The potential flow over an oscillating elliptic cylinder in a free-stream was obtained from a form of the complex velocity potential similar to that given by Kochin[9]. The complex potential used in the present analysis and given by

$$w = \frac{U}{\zeta}\left[b\cos\alpha + i\,a\sin\alpha\right] - \frac{i\Omega_z'(a^2 - b^2)}{4\zeta^2} - \frac{\Gamma'}{2\pi i}\log\zeta \tag{1}$$

was obtained by mapping the flow about a circular cylinder onto that around an elliptic cylinder. With standard potential flow procedures and by letting

$$u_\delta = \frac{u_\delta'}{U}\,,\quad \Gamma = \frac{\Gamma'}{2\pi UL}\,,\quad \Omega_z = \frac{\Omega_z' L}{U}\,,$$

the inviscid flow about an oscillating infinite elliptic cylinder was found to be:

$$u_\delta(x,t) = \frac{1}{R}\left[(1+\beta)\sin(\eta - \alpha(t)) + \Gamma(t)\right] + \frac{\Omega_z}{2R}\left[(1-\beta^2)\cos 2\eta + 2\beta\right] \tag{2}$$

$$\text{where } R = (\sin^2\eta + \beta^2\cos^2\eta)^{1/2}$$

The potential flow for a stationary elliptic cylinder in an oscillatory stream may be obtained from equation (2) by omitting the term containing Ω_z. The resulting expression for $u_\delta(x,t)$ is then identical with that studied by Moore[7] in his analysis of dynamic stall. The angle-of-attack and the circulation are each functions of time and are assumed to have the following forms:

$$\alpha(t) = \alpha_o + \Delta\alpha \sin \omega t \tag{3}$$

$$\Gamma(t) = \Gamma_o + \Gamma_{10}\, \Delta\alpha \cos \omega t + \Gamma_{11}\, \Delta\alpha \sin \omega t \tag{4}$$

where $\Delta\alpha$ is a constant perturbation of the incidence angle. The pitch rate, Ω_z, is given by

$$\Omega_z = - \dot{\alpha}(t) = - \omega\, \Delta\alpha \cos \omega t \tag{5}$$

The expression for $\Gamma(t)$ is the sum of sine and cosine components, thus permitting phase lead and lag in the final expression for circulation. Substituting (3) and (4) into (2) and discarding terms of order $(\Delta\alpha)^2$ or higher yields:

$$u_\delta(x,t) = u_{\delta_o}(x) + u_{\delta_{10}}(x)\Delta\alpha \cos \omega t + u_{\delta_{11}}(x)\Delta\alpha \sin \omega t \tag{6}$$

where:

$$u_{\delta_o} = \frac{(1 + \beta)\sin(\eta - \alpha_o) + \Gamma_o}{R} \tag{7}$$

$$u_{\delta_{10}} = \frac{\Gamma_{10} - \omega\beta - \frac{\omega(1 - \beta^2)}{2}\cos 2\eta}{R} \tag{8}$$

$$u_{\delta_{11}} = \frac{\Gamma_{11} - (1 + \beta)\cos(\eta - \alpha_o)}{R} \tag{9}$$

The boundary layer streamwise coordinate, x, is related to the angular measure, η, by

$$dx/d\eta = - R(\eta)/2.$$

Governing Equations

The non-dimensional, unsteady, laminar boundary layer equations for incompressible flow in a moving coordinate system, provided frequency is sufficiently small, are given by:

$$\frac{\partial u}{\partial x} + \frac{\partial v}{\partial y} = 0 \tag{10}$$

$$\frac{\partial u}{\partial t} + u \frac{\partial u}{\partial x} + v \frac{\partial u}{\partial y} = \frac{\partial u_\delta}{\partial t} + u_\delta \frac{\partial u_\delta}{\partial x} + \frac{\partial^2 u}{\partial y^2} \tag{11}$$

with boundary conditions

$$u(x,0,t) = 0 \ , \ v(x,0,t) = 0$$

$$\lim_{y \to \infty} u(x,y,t) = u_\delta(x,t). \tag{12}$$

Physically, the points of boundary layer separation on the upper and lower surfaces move back and forth with time as the body oscillates. The present analysis accounts for this effect by transforming the boundary layer equations (10) and (11) with a scaling of the x-coordinate so that separation always occurs at a constant value of the streamwise coordinate in the new system. Before development of this transformation, a brief discussion of the nature of *unsteady separation seems necessary.*

Moore[10], Rott[11], and Sears[8], all noted that vanishing of the wall shear does not necessarily imply separation in unsteady boundary layer flow. Instead, they independently postulated a model (known as the MRS model) in which the unsteady separation point is characterized by the simultaneous vanishing of the shear and the velocity at some point, usually away from the wall, as seen by an observer moving with the separation point. The exact implications of this definition of unsteady separation on the analytical prediction of separation point location is not known. However, Crimi[5] indicates that for typical helicopter rotor Reynolds Number and dimensionless

pitch rate, the difference between streamwise location of the separation point as given by the MRS model and the location of the classical point of vanishing wall shear is approximately 0.6 percent of the airfoil chord. This result, in addition to the physical reality that as pitch rate approaches zero, the streamwise location of unsteady and steady separation points must coincide, leads to the adoption of vanishing wall shear as adequately defining the location of separation. Even though in the strict sense this definition is inaccurate, for the lower range of pitch rates under consideration here this criterion is well within the accuracy of an analysis to order $\Delta\alpha$.

To scale the x-coordinate, the new streamwise coordinate, ξ, is given by

$$\xi = xq(t) \tag{13}$$

where q(t) is some function to be determined which adjusts the streamwise distance so that separation always occurs at a constant value of ξ. With this scaling, the governing equations (10), (11), and boundary conditions (12) become:

$$q\frac{\partial u}{\partial \xi} + \frac{\partial v}{\partial y} = 0 \tag{14}$$

$$\frac{\partial u}{\partial t} + \frac{\xi \dot{q}}{q}\frac{\partial u}{\partial \xi} + uq\frac{\partial u}{\partial \xi} + v\frac{\partial u}{\partial y} = \frac{\xi \dot{q}}{q}\frac{\partial u_\delta}{\partial \xi} + \frac{\partial u_\delta}{\partial t} + qu_\delta\frac{\partial u_\delta}{\partial \xi} + \frac{\partial^2 u}{\partial y^2} \tag{15}$$

$$u(\xi,0,t) = 0,\ v(\xi,0,t) = 0$$

$$\lim_{y\to\infty} u(\xi,y,t) = u_\delta(\xi,t) \tag{16}$$

In a procedure completely analogous with steady boundary layers, equations (14) and (15) may be written in terms of integral relations as follows:

$$\tau_w = \frac{\partial}{\partial t}(\delta^* u_\delta) + \frac{\xi \dot{q}}{q}\frac{\partial}{\partial \xi}(\delta^* u_\delta) + q\frac{\partial}{\partial \xi}(\theta u_\delta^2) + q u_\delta \delta^* \frac{\partial u_\delta}{\partial \xi} \tag{17}$$

where:

$$\delta^* = \int_0^\delta (1 - \frac{u}{u_\delta})dy \tag{18}$$

$$\theta = \int_0^\delta \frac{u}{u_\delta}(1 - \frac{u}{u_\delta})dy \tag{19}$$

$$\tau_w = \left.\frac{\partial u}{\partial y}\right|_{y=0} \tag{20}$$

The solution technique employed in this work resembles a procedure used by Teipel[12] to solve the classical unsteady momentum integral equation. To extend the range of pressure gradients for which this procedure is applicable, the present work utilizes a fifth order polynomial, similar to that of Dryden[13] to obtain an additional degree of freedom in choosing the polynomial coefficients. Thus, the general form of the u-component of boundary layer velocity was assumed as

$$\begin{aligned} u(\xi,y,t) &= a_o + b_o r + c_o r^2 + d_o r^3 + e_o r^4 + h_o r^5 \\ &+ \Delta\alpha \cos \omega t \,[a_{10} + b_{10} r + C_{10} r^2 + d_{10} r^3 + e_{10} r^4 + h_{10} r^5] \\ &+ \Delta\alpha \sin \omega t \,[a_{11} + b_{11} r + c_{11} r^2 + d_{11} r^3 + e_{11} r^4 + h_{11} r^5] \end{aligned} \tag{21}$$

where

$$r = y/\delta(\xi,t) \tag{22}$$

The coefficients in equation (21) are determined by matching the following conditions on the wall and at the outer edge of the boundary layer:

$$y = 0 : u = 0 \text{ and } \frac{\partial^2 u}{\partial y^2} = -\left(\frac{\partial u_\delta}{\partial t} + \frac{\xi \dot{q}}{q}\frac{\partial u_\delta}{\partial \xi} + q u_\delta \frac{\partial u_\delta}{\partial \xi}\right)$$

$$y = \delta : u = u_\delta \,,\ \frac{\partial u}{\partial y} = 0 \,,\ \text{and } \frac{\partial^2 u}{\partial y^2} = 0 \tag{23}$$

The scaling function q(t) was chosen to be of the following general form:

$$q(t) = 1 + \Delta\alpha\, q_1(t) = 1 + C_1\, \Delta\alpha \cos \omega t + C_2\, \Delta\alpha \sin \omega t. \tag{24}$$

In this form, C_1 and C_2 are to be determined such that, to order $\Delta\alpha$, the separation point always occurs at a constant value of ξ. Also, an unsteady shape factor, λ, is defined to be:

$$\lambda = \delta^2 \left[\frac{1}{u_\delta} \frac{\partial u_\delta}{\partial t} + \frac{\dot{\xi q}}{q u_\delta} \frac{\partial u_\delta}{\partial \xi} + q \frac{\partial u_\delta}{\partial \xi}\right] . \tag{25}$$

The unsteady boundary layer thickness, $\delta(\xi,t)$, was assumed to be of the form

$$\delta(\xi,t) = \delta_o(\xi) + \delta_{10}(\xi)\Delta\alpha \cos \omega t + \delta_{11}(\xi)\Delta\alpha \sin \omega t \tag{26}$$

where $\delta_o(\xi)$ is given by the steady-state analysis and $\delta_{10}(\xi)$ and $\delta_{11}(\xi)$ are determined from the unsteady solution. Substituting gives the shape factor in expanded form as:

$$\lambda = \lambda_o + \lambda_{10}\, \Delta\alpha \cos \omega t + \lambda_{11}\, \Delta\alpha \sin \omega t \tag{27}$$

$$\lambda_o = \delta_o^2 \frac{du_{\delta_0}}{d\xi} \tag{28}$$

$$\lambda_{10} = \delta_o^2 \frac{du_{\delta_{10}}}{d\xi} + \delta_o^2 \omega \frac{u_{\delta_{11}}}{u_{\delta_0}} - \delta_o^2 C_1 \xi \frac{d^2 u_{\delta_0}}{d\xi^2} + 2\delta_o \delta_{10} \frac{du_{\delta_0}}{d\xi} \tag{29}$$

$$\lambda_{11} = \delta_o^2 \frac{du_{\delta_{11}}}{d\xi} - \delta_o^2 \omega \frac{u_{\delta_{10}}}{u_{\delta_0}} - \delta_o^2 C_2 \xi \frac{d^2 u_{\delta_0}}{d\xi^2} + 2\delta_o \delta_{11} \frac{du_{\delta_0}}{d\xi} \tag{30}$$

Recall that u_{δ_o}, $u_{\delta_{10}}$, and $u_{\delta_{11}}$ were given as functions of x only; however, the problem solution occurs in the (ξ,y,t) coordinate system. To obtain values of any component of the potential flow, u_δ, corresponding to a particular ξ, the increment form of Taylor's Series is applied. For example, consider the expansion for $u_{\delta_o}(x)$ given below:

$$u_{\delta_o}(x) = u_{\delta_o}\left(\frac{\xi}{1 + \Delta\alpha\, q_1}\right) \simeq u_{\delta_o}(\xi(1 - \Delta\alpha\, q_1))$$

$$\simeq u_{\delta_o}(\xi) - \Delta\alpha\, \xi\, q_1 \frac{du_{\delta_0}}{d\xi} \tag{31}$$

Matching the boundary conditions gives the following form for the velocity profile.

$$\frac{u}{u_\delta(\xi,t)} = F(b_1,r) + \lambda\, G(b_2,r) \tag{32}$$

where

$$F(b_1,r) = b_1 r + (10 - 6b_1)r^3 + (8b_1 - 15)r^4 + (6 - 3b_1)r^5 \tag{33}$$

$$G(b_2,r) = b_2 r - \frac{1}{2}r^2 + (\frac{3}{2} - 6b_2)r^3 + (8b_2 - \frac{3}{2})r^4 + (\frac{1}{2} - 3b_2)r^5 \tag{34}$$

In equation (32), the coefficient of r, $b_1 + \lambda b_2$, may be arbitrarily chosen so as to increase the range of λ_o for which the method is valid. Dryden[13] chose $b_1 = 1.89$ and $b_2 = 0.11$ for his analysis. However, for the present work values of $b_1 = 17/9$ and $b_2 = 1/7$ were chosen because, when compared with Dryden's choices, the resulting steady lift curve showed less deviation from that obtained by the classical method, yet increasing the valid range of λ_o. Thus u/u_δ may be written as

$$\frac{u}{u_\delta} = F(r) + \lambda_o G(r) + \lambda_{10} G(r)\, \Delta\alpha \cos \omega t + \lambda_{11}\, G(r)\, \Delta\alpha \sin \omega t \tag{35}$$

where

$$F(r) = \frac{17}{9}r - \frac{4}{3}r^3 + \frac{1}{9}r^4 + \frac{1}{3}r^5$$

$$G(r) = \frac{1}{7}r - \frac{1}{2}r^2 + \frac{9}{14}r^3 - \frac{5}{14}r^4 + \frac{1}{14}r^5$$

The model for the boundary layer velocity can accommodate time varying phase shifts and reverse flow.

Using the velocity profile (35), the integral relations may be expanded as follows:

$$\delta^* = \delta_o^* + \delta_{10}^* \Delta\alpha \cos \omega t + \delta_{11}^* \Delta\alpha \sin \omega t \tag{36}$$

$$\theta = \theta_o + \theta_{10} \Delta\alpha \cos \omega t + \theta_{11} \Delta\alpha \sin \omega t \tag{37}$$

$$\tau_w = \tau_{w_o} + \tau_{w_{10}} \Delta\alpha \cos \omega t + \tau_{w_{11}} \Delta\alpha \sin \omega t \tag{38}$$

where

$$\tau_{w_o} = \frac{u_{\delta_0}}{\delta_0}\left(\frac{17}{9} + \frac{\lambda_o}{7}\right)$$

$$\tau_{w_{10}} = \frac{u_{\delta_0}}{\delta_0}\left[\frac{\lambda_{10}}{7} + \left(\frac{17}{9} + \frac{\lambda_o}{7}\right)\left(\frac{u_{\delta_{10}}}{u_{\delta_0}} - \frac{\delta_{10}}{\delta_0}\right)\right]$$

$$\tau_{w_{11}} = \frac{u_{\delta_0}}{\delta_0}\left[\frac{11}{7} + \left(\frac{17}{9} + \frac{\lambda_o}{7}\right)\left(\frac{u_{\delta_{11}}}{u_{\delta_0}} - \frac{\delta_{11}}{\delta_0}\right)\right]$$

Substituting into equation (17) and discarding terms of order $(\Delta\alpha)^2$ or larger yields the following set of governing equations:

<u>order $(\Delta\alpha)^0$:</u>

$$(2\theta_o + \delta_0^*)\frac{du_{\delta_0}}{d\xi} + u_{\delta_0}\frac{d\theta_0}{d\xi} = \frac{\tau_{w_0}}{u_{\delta_0}} \tag{39}$$

order $(\Delta\alpha)^1$:

$$\frac{d\delta_{10}}{d\xi} Q_1 + \delta_{10}Q_2 + \delta_{11}Q_3 + C_1Q_4 + C_2Q_5 - \omega \frac{du_{\delta_{11}}}{d\xi} Q_6$$

$$+ \frac{du_{\delta_{10}}}{d\xi} Q_7 + u_{\delta_{10}} Q_8 + \omega u_{\delta_{11}} Q_9 - \frac{d^2u_{\delta_{10}}}{d\xi^2} Q_{10} = 0 \qquad (40)$$

$$\frac{d\delta_{11}}{d\xi} Q_1 + \delta_{11}Q_2 - \delta_{10}Q_3 - C_1Q_5 + C_2Q_4 + \omega \frac{du_{\delta_{10}}}{d\xi} Q_6$$

$$+ \frac{du_{\delta_{11}}}{d\xi} Q_7 + u_{\delta_{11}} Q_8 - \omega u_{\delta_{10}} Q_9 - \frac{d^2u_{\delta_{11}}}{d\xi^2} Q_{10} = 0 \qquad (41)$$

where

$$Q_1 = \frac{u_{\delta_0}}{693} \left[\frac{33707}{405} - \frac{1329}{2520} \lambda_0 - \frac{10}{49} \lambda_0^2\right]$$

$$Q_2 = \frac{1}{693} \left[\frac{2(372711)}{405} - \frac{11281}{840} \lambda_0 - \frac{20}{49} \lambda_0^2\right] \frac{du_{\delta_0}}{d\xi}$$

$$+ \frac{1}{\delta_0^2} \left(\frac{17}{9} + \frac{\lambda_0}{7}\right) - \frac{u_{\delta_0}}{693} \left(\frac{1329}{2520} + \frac{20}{49} \lambda_0\right) \frac{d\lambda_0}{d\xi}$$

$$Q_3 = \omega\left[\frac{14}{45} - \frac{\lambda_0}{56}\right]$$

$$Q_4 = - \frac{\xi}{\delta_0 u_{\delta_0}} \frac{du_{\delta_0}}{d\xi} \left(\frac{17}{9} + \frac{\lambda_0}{7}\right) + u_{\delta_0} \frac{d\theta_0}{d\xi} \left(1 - \frac{\xi}{u_{\delta_0}} \frac{du_{\delta_0}}{d\xi}\right)$$

$$+\frac{u_{\delta_0}\delta_0^3}{693}\left(\frac{443}{2520}+\frac{4}{49}\lambda_0\right)\frac{d^3u_{\delta_o}}{d\xi^3}+\delta_0\frac{d^2u_{\delta_0}}{d\xi^2}\left[\xi\left(\frac{1}{7}+\frac{11281}{(693)\ (2520)}\lambda_0\right.\right.$$

$$\left.+\frac{8}{(693)\ (49)}\lambda_0^2\right)+\frac{u_{\delta_0}\delta_0^2}{693}\left(\frac{443}{2520}+\frac{4}{49}\lambda_0+\frac{4}{49}\xi\frac{d\lambda_o}{d\xi}\right)\Big]$$

$$+\xi\frac{d^2u_{\delta_0}}{d\xi^2}\left[\frac{u_{\delta_0}\delta_0^2}{231}\frac{d\delta_o}{d\xi}\left(\frac{443}{2520}+\frac{4}{49}\lambda_o\right)-(2\theta_o+\delta_0^*)\right]$$

$$Q_5=\omega\left[\frac{\delta_0^3\xi}{168}\frac{d^2u_{\delta_o}}{d\xi^2}+\frac{d\delta_0^*}{d\xi}\right]$$

$$Q_6=\frac{\delta_0^3}{693}\left[\frac{5419}{1260}+\frac{4}{49}\lambda_o\right]$$

$$Q_7=2\theta_o+\delta_0^*\,\delta_0\left(\frac{1}{7}+\frac{11281}{(693)(2520)}\lambda_o+\frac{8}{(693)(49)}\lambda_0^2\right)$$

$$-\frac{u_{\delta_0}\delta_0^2}{231}\left(\frac{443}{2520}+\frac{4}{49}\lambda_o\right)\frac{d\delta_0}{d\xi}-\frac{4}{(693)(49)}u_{\delta_0}\delta_0^3\frac{d\lambda_o}{d\xi}$$

$$Q_8=\frac{\omega^2}{168}\frac{\delta_0^3}{u_{\delta_0}}+\frac{d\theta_o}{d\xi}$$

$$Q_9=\frac{\delta_0}{u_{\delta_o}}\left[\frac{53}{315}-\frac{21233}{(1386)(1260)}\lambda_o-\frac{4}{(693)(49)}\lambda_0^2\right.$$

$$\left.-\frac{\delta_0}{231}u_{\delta_0}\frac{d\delta_0}{d\xi}\left(\frac{443}{2520}+\frac{4}{49}\lambda_0\right)-\frac{4}{(693)(49)}u_{\delta_0}\delta_0^2\frac{d\lambda_o}{d\xi}\right]$$

$$Q_{10}=\frac{u_{\delta_0}\delta_0^3}{693}\left(\frac{443}{2520}+\frac{4}{49}\lambda_o\right)$$

Note that each of the Q_i's is a function of the steady-state solution only.

In the governing equations, (40) and (41), values for C_1 and C_2 are undetermined. In order for q(t) to properly adjust the x-coordinate C_1 and C_2 must be calculated from two auxiliary relations. These relations are obtained by examining the unsteady shear given by equation (38). The steady separation is defined as the point for which τ_{w_o} vanishes or equivalently where $\lambda_o = -7(17)/9$. Thus for total τ_w to vanish at this point for all time, $\tau_{w_{10}}$ and $\tau_{w_{11}}$ must also simultaneously vanish at this point. This occurs when both λ_{10} and λ_{11} are zero at the separation point. Thus equations (29) and (30) give:

$$\lambda_{10}(\xi_s) = \left| \delta_0^2 \frac{du_{\delta_{10}}}{d\xi} + \delta_0^2 \omega \frac{u_{\delta_{11}}}{u_{\delta_0}} - \delta_0^2 C_1 \xi \frac{d^2 u_{\delta_0}}{d\xi^2} + 2\delta_0 \delta_{10} \frac{du_{\delta_o}}{d\xi} \right|_{\xi=\xi_s} = 0 \qquad (42)$$

$$\lambda_{11}(\xi_s) = \left| \delta_0^2 \frac{du_{\delta_{11}}}{d\xi} - \delta_0^2 \omega \frac{u_{\delta_{10}}}{u_{\delta_0}} - \delta_0 C_2 \xi \frac{d^2 u_{\delta_0}}{d\xi^2} + 2\delta_0 \delta_{11} \frac{du_{\delta_o}}{d\xi} \right|_{\xi=\xi_s} = 0 \qquad (43)$$

From equations (42) and (43), C_1 and C_2 may be calculated such that q(t) properly scales the physical x-coordinate.

CIRCULATION CRITERION

Determination of the appropriate potential flow about the oscillating body involves specifying correct values of the unsteady circulation components in equation (6). The criterion used in the present study to determine values of Γ_o, Γ_{10}, and Γ_{11} was advanced by Sears[8]. Sears points out that his criterion is an extension of the earlier work by Howarth[14] based on a theorem developed by Taylor[15]. The Taylor-Howarth Criterion for determining

the proper circulation was the condition that the net vorticity shed into the wake from both the upper and lower surfaces must be zero. Sears' modification of this requirement to account for unsteady effects, known as the revised Taylor-Howarth criterion, is given by:

$$\frac{d\Gamma}{dt} = \text{rate of vorticity flux into the wake} \tag{44}$$

Allowing for the movement of the separation points, the criterion in (44) becomes

$$\frac{d\Gamma}{dt} = \frac{1}{2}\,\bar{u}_{\delta}^{2} - \frac{1}{2}\,\underline{u}_{\delta}^{2} + \underline{u}_{\delta}\,\frac{d\underline{x}_s}{dt} - \bar{u}_{\delta}\,\frac{d\bar{x}_s}{dt} \tag{45}$$

where the upper and lower bars denote conditions at separation on the upper and lower surfaces of the body, respectively. Changing the criterion in equation (45) to the (ξ,y,t) coordinate system yields the following three restrictions on Γ_0, Γ_{10}, and Γ_{11} when coefficients of 1, $\Delta\alpha \cos \omega t$, and $\Delta\alpha \sin \omega t$ are equated:

$$\bar{u}_{\delta_0}^{2} = \underline{u}_{\delta_0}^{2} \tag{46}$$

$$T_1 = \omega\Gamma_{11} - \bar{u}_{\delta_0}\,\bar{u}_{\delta_{10}} + \bar{\xi}_s\bar{C}_1\,\bar{u}_{\delta_0}\left.\frac{du_{\delta_0}}{d\xi}\right|_{\xi=\bar{\xi}_s} - \bar{C}_2\,\bar{\xi}_s\omega\bar{u}_{\delta_0}$$

$$+ \underline{u}_{\delta_0}\,\underline{u}_{\delta_{10}} - \underline{\xi}_s\,\underline{C}_1\,\underline{u}_{\delta_0}\left.\frac{du_{\delta_0}}{d\xi}\right|_{\xi=\underline{\xi}_s} + \underline{C}_2\,\underline{\xi}_s\,\omega\underline{u}_{\delta_0} = 0 \tag{47}$$

$$T_2 = -\omega\Gamma_{10} - \bar{u}_{\delta_0}\,\bar{u}_{\delta_{11}} + \bar{\xi}_s\,\bar{C}_2\,\bar{u}_{\delta_0}\left.\frac{du_{\delta_0}}{d\xi}\right|_{\xi=\xi_s} + \bar{C}_1\,\bar{\xi}_s\omega\bar{u}_{\delta_0}$$

$$+ \underline{u}_{\delta_0}\,\underline{u}_{\delta_{11}} - \underline{\xi}_s\,\underline{C}_2\,\underline{u}_{\delta_0}\left.\frac{du_{\delta_0}}{d\xi}\right|_{\xi=\underline{\xi}_s} - \underline{C}_1\,\underline{\xi}_s\omega\underline{u}_{\delta_0} = 0 \qquad (48)$$

From equation (46), Γ_o is determined by iteration until the velocity at the upper and lower separation points have equal magnitudes. To obtain correct values for the unsteady components of circulation, iteration is performed simultaneously on both Γ_{10} and Γ_{11} until equations (47) and (48) are satisfied.

SOLUTION PROCEDURE

To solve for the steady solution, let $Z = \delta_0^2$, then equation (39) may be written in the following form:

$$\frac{dZ}{d\xi} = \frac{g(\lambda_o)}{u_{\delta_0}} + Z^2\,\frac{d^2u_{\delta_o}}{d\xi^2}\,h(\lambda_o) \qquad (49)$$

where $g(\lambda_o)$ and $h(\lambda_o)$ are as follows:

$$g(\lambda_o) = \frac{-3.7777 + .81690\,\lambda_o - .1292\,\lambda_o^2 - .00023559\,\lambda_o^3}{-.120097 + .00076101\,\lambda_o + .00029449\,\lambda_o^2}$$

$$h(\lambda_o) = \frac{-.00050734 - .00023559\,\lambda_o}{-.120097 + .00076101\,\lambda_o + .00029449\,\lambda_o^2}$$

At the stagnation point u_{δ_o} is zero, thus requiring that the numerator of $g(\lambda_o)$ also vanish here. The physically realistic value of λ_o for which $g(\lambda_o)$ becomes zero is $\lambda_o = 5.0684$. Using the initial condition obtained from applying l' Hospital's rule, equation (49) is integrated from the stagnation point to the point on each surface where τ_{w_o} first vanishes. The corresponding values of u_{δ_o} were determined and the criterion of equation (46) was checked to decide if

the proper value of Γ_o had been chosen. The process is repeated until the proper value of Γ_o is found.

The unsteady solution is governed by the linear differential equations, (40) and (41), which contain the unknown constants C_1 and C_2 in addition to $u_{\delta_{10}}$ and $u_{\delta_{11}}$.

Correct values of Γ_{10} and Γ_{11}, which fully specify $u_{\delta_{10}}$ and $u_{\delta_{11}}$ along the body surface, must be determined iteratively. The linearity of the governing equations permits each of the unknowns, δ_{10} and δ_{11}, to be expressed as a sum of three components as follows:

$$\delta_{10} = {}^1\delta_{10} + C_1\ {}^2\delta_{10} + C_2\ {}^3\delta_{10}$$

$$\delta_{11} = {}^1\delta_{11} + C_1\ {}^2\delta_{11} + C_2\ {}^3\delta_{11}$$

Substitution for δ_{10} and δ_{11} into equations (40) and (41) permits the pair of governing equations to be split into three sets of two equations each by equating coefficients of 1, C_1, and C_2. These new governing equations become:

$$\frac{d\,{}^1\delta_{10}}{d\xi} Q_1 + {}^1\delta_{10}\, Q_2 + {}^1\delta_{11}\, Q_3 - \omega \frac{du_{\delta_{11}}}{d\xi} Q_6 + \frac{du_{\delta_{10}}}{d\xi} Q_7 + u_{\delta_{10}} Q_8 + \omega u_{\delta_{11}} Q_9 - \frac{d^2 u_{\delta_{10}}}{d\xi^2} Q_{10} = 0 \qquad (50a)$$

$$\frac{d\,{}^1\delta_{11}}{d\xi} Q_1 + {}^1\delta_{11}\, Q_2 - {}^1\delta_{10}\, Q_3 + \omega \frac{du_{\delta_{10}}}{d\xi} Q_6 + \frac{du_{\delta_{11}}}{d\xi} Q_7 + u_{\delta_{11}} Q_8 - \omega u_{\delta_{10}} Q_9 - \frac{d^2 u_{\delta_{11}}}{d\xi^2} Q_{10} = 0 \qquad (50b)$$

$$\frac{d^2\delta_{10}}{d\xi} Q_1 + {}^2\delta_{10}\, Q_2 + {}^2\delta_{11}\, Q_3 + Q_4 = 0 \qquad (51a)$$

$$\frac{d^2\delta_{11}}{d\xi} Q_1 + {}^2\delta_{11}\, Q_2 - {}^2\delta_{10}\, Q_3 - Q_5 = 0 \qquad (51b)$$

$$\frac{d^3\delta_{10}}{d\xi} Q_1 + {}^3\delta_{10}\, Q_2 + {}^3\delta_{11}\, Q_3 + Q_5 = 0 \qquad (52a)$$

$$\frac{d^3\delta_{11}}{d\xi} Q_1 + {}^3\delta_{11}\, Q_2 - {}^3\delta_{10}\, Q_3 + Q_4 = 0 \qquad (52b)$$

Note that equations (51) and (52) contain only input from the steady solution and may be solved independently of the iterative process necessary to determine Γ_{10} and Γ_{11}. Thus only equations (50), which are solved last, depend on the choices of Γ_{10} and Γ_{11}.

Since Q_1 vanishes at the stagnation point, the initial values of ${}^2\delta_{10}$ and ${}^2\delta_{11}$ may be calculated by solving the two algebraic equations obtained by requiring the last three terms of equations (51a) and (51b) to be zero at the stagnation point. Similarly, initial values of ${}^3\delta_{10}$ and ${}^3\delta_{11}$ are obtained from equations (52a) and (52b). Initial values for the derivatives of these four unknowns are obtained by applying l'Hospital's rule to each pair of equations and solving the resulting algebraic relations. Equations (51) and (52) are integrated by Runge-Kutta techniques from the stagnation point around the upper and lower surfaces until the points of steady-state separation are reached. Values of the variables at the separation points are determined and retained for later use when calculating the scaling coefficients, C_1 and C_2, on each surface.

The iterative portion of the unsteady solution must be solved for each set of Γ_{10} and Γ_{11}. Once again initial values for ${}^1\delta_{10}$ and ${}^1\delta_{11}$ are needed in order

to start the integration process. However, the above procedure of simply applying 1'Hospital's rule and then solving the resulting simultaneous equations is not possible. The physical reality of a moving stagnation point (i.e., $u_{\delta_{10}}$ and $u_{\delta_{11}}$ may be non-zero at the point on the body for which u_{δ_0} vanishes) prevents use of equations (50) to calculate initial values at the stagnation point. Close examination of equations (50) reveals that both Q_8 and Q_9 are unbounded when u_{δ_0} is zero. Consequently, unless the prescribed potential flow components, $u_{\delta_{10}}$ and $u_{\delta_{11}}$, also vanished at the steady-state stagnation point, 1'Hospital's rule would not be applicable.

In the present study, the unsteady stagnation point was treated in a manner similar to that used by Rott[11]. Once a solution was obtained for the stagnation region, initial values of ${}^1\delta_{10}$ and ${}^1\delta_{11}$ at a small distance on either side of the stagnation point were calculated by matching the shape of velocity profiles resulting from Rott's procedure with those used in the unsteady momentum integral technique. Experience showed that the choice of initial values for ${}^1\delta_{10}$ and ${}^1\delta_{11}$ was not cirtical because boundary layers initially behave in an almost similar fashion. Thus, any reasonable choice of starting values for ${}^1\delta_{10}$ and ${}^1\delta_{11}$ gives identical results after integrating downstream to the separation region. Equations (50) are integrated over each surface of the body to the steady separation point and values of ${}^1\delta_{10}$ and ${}^1\delta_{11}$ at each separation point are obtained for use in calculating C_1 and C_2 on each surface.

To solve for C_1 and C_2, δ_{10} and δ_{11} are substituted into equations (42) and (43) and grouped to give:

$$\left| \frac{2\,{}^2\delta_{10}}{\delta_0} \frac{du_{\delta_0}}{d\xi} - \xi \frac{d^2u_{\delta_0}}{d\xi^2} \right|_{\xi=\xi_s} C_1 + \left| \frac{2\,{}^3\delta_{10}}{\delta_0} \frac{du_{\delta_0}}{d\xi} \right|_{\xi=\xi_s} C_2$$

$$+ \left| \frac{du_{\delta_{10}}}{d\xi} + \frac{u_{\delta_{11}}}{u_{\delta_0}} + \frac{2\,{}^1\delta_{10}}{\delta_0} \frac{du_{\delta_0}}{d\xi} \right|_{\xi=\xi_s} = 0 \qquad (53)$$

$$\left| \frac{2}{\delta_0} \frac{^2\delta_{11}}{} \frac{du_{\delta_0}}{d\xi} \right|_{\xi=\xi_s} C_1 + \left| \frac{2}{\delta_0} \frac{^3\delta_{11}}{} \frac{du_{\delta_0}}{d\xi} - \xi \frac{d^2u_{\delta_0}}{d\xi^2} \right|_{\xi=\xi_s} C_2$$

$$+ \left| \frac{du_{\delta_{11}}}{d\xi} - \omega \frac{u_{\delta_{10}}}{u_{\delta_0}} + \frac{2}{\delta_0} \frac{^1\delta_{11}}{} \frac{du_{\delta_0}}{d\xi} \right|_{\xi=\xi_s} = 0 \qquad (54)$$

Once values of C_1 and C_2 are obtained, the unsteady circulation criterion is used to decide if correct values were chosen for Γ_{10} and Γ_{11}. If either T_1 or T_2, equations (47) and (48), are significantly different from zero, then new values of Γ_{10} and Γ_{11} are chosen and the solution repeated until T_1 and T_2 are both approximately zero. Prediction of new values for Γ_{10} and Γ_{11} is rather straightforward after the results of T_1 and T_2 from two trial values are obtained. Since T_1 is very sensitive to changes in Γ_{10} and insensitive to changes in Γ_{11} and T_2 exhibits just the opposite behavior, linear extrapolation is quite adequate for determining new trial values of Γ_{10} and Γ_{11}.

Upon completion of the above procedure, the unsteady circulation has been determined for the body oscillating at a particular frequency about some mean angle-of-attack.

DISCUSSION OF RESULTS

Once the components of total circulation have been determined, the two-dimensional lift coefficient is then obtained from the following expression relating circulation and lift:

$$C_\ell(t) = 2\pi\Gamma(t)$$

A plot of steady lift coefficient as a function of angle-of-attack was formed by repeatedly solving the governing steady-state equations for various α_o and is presented in Figure 2. A summary of steady-state results for several angles

Table 1. Summary of results from the steady-state solutions

α_0	Γ_0	$\bar{\xi}_s$	$\underline{\xi}_s$
2^0	0.0250	0.8941	-0.9502
6^0	0.0695	0.7399	-0.9747
8^0	0.0800	0.5259	-0.9836
9^0	0.0750	0.3427	-0.9892

of-attack is presented in Table 1. Corresponding to a particular α_o, Table 1 gives the steady component of circulation and the location of the separation point on both the top and bottom surfaces.

Once the steady-state results are available as input, the unsteady governing equations are solved for a nominal angle-of-attack, α_o, and a particular frequency, ω. Even though the unsteady governing equations are independent of $\Delta\alpha$, its magnitude is restricted by the assumption that terms of second order or higher are negligible. Thus, for the time dependent results presented herein, $\Delta\alpha$ is chosen to be one-half degree. For the larger values of α_o, an increased $\Delta\alpha$ would be permissible.

The unsteady results for a range of mean angles-of-attack and frequencies are presented in Table 2. Notice that Table 2 includes the scaling coefficients, C_1 and C_2 in equation (23), for both the upper and lower surfaces. Also the resulting nonsteady components of the total circulation, Γ_{10} and Γ_{11}, are given for each α_o and frequency. Using the value of Γ_o from Table 1 and values of Γ_{10} and Γ_{11} from Table 2 corresponding to a particular α_o and ω, the unsteady

Table 2. Summary of results from the unsteady solutions

α_0	ω	$\bar{C}_1$	$\bar{C}_2$	C_{-1}	C_{-2}	Γ_{10}	Γ_{11}
2^0	0.10	0.0666	1.4501	- .07900	- .6665	- .0231	0.7209
6^0	0.10	- .3989	5.4978	- .07361	- .4304	- .0712	0.4958
8^0	0.01	- .3372	18.975	- .00545	- .4483	- .0093	- 0.0837
	0.10	- 3.293	18.446	- .05350	- .4541	- .0899	- 0.1018
	0.30	- 8.264	14.907	- .14000	- .4916	- .2054	- .2197
9^0	0.01	- 1.010	44.466	- .00033	- .5325	0.0061	- 1.0952
	0.10	- 9.752	42.634	- .00324	- .5334	0.0614	- 1.0993
	0.30	-22.85	31.481	- .00796	- .5395	0.1921	- 1.126

circulation anf lift coefficients may be easily constructed. In Figure 3 lift hysteresis loops for the oscillating elliptic cylinder corresponding to several nominal angles-of-attack are presented. The effect of periodic incidence changes about differing values of α_o is apparent. Note that for $\alpha_o = 2^0$, the loop is very thin and proceeds in a counterclockwise direction. The results at $\alpha_o = 6^0$ are very similar with the loop progressing in the same direction but becoming thicker as the region near $C_{\ell_{max}}$, where the viscous effects are more prevalent, is approached. For $\alpha_o = 8^0$, approximately the angle-of-attack for steady $C_{\ell_{max}}$, the loop is thickening but continues to exhibit the counterclockwise direction. In the steady-state stall region at $\alpha_o = 9^0$, the significant difference is that the loop has changed directions and now proceeds in a clockwise manner making the direction of the hysteresis loop change as α_o is increased from the low angles-of-attack. This behavior, however, is not completely unexpected as evidenced by the experimental

results of Liiva et al[2] and presented here as Figure 4. The results presented in Figure 4 were obtained from two-dimensional tests of a cylinder of airfoil cross section periodically oscillating with an angle-of-attack increment of about five degrees. Even though the theoretical results of Figure 3 are obtained for an elliptic cylinder using an analysis to order $\Delta\alpha$ only, a comparison with the experimental results of Figure 4 is enlightening. Notice that the direction of the experimental hysteresis loops in Figure 4 also change from counterclockwise to clockwise when α_o is increased, as do those of Figure 3. The major difference however is where this direction change occurs. In the experimental results, the loop direction change is indicated by a figure eight behavior in the hysteresis loop at an α_o prior to that for steady maximum lift. However, in the present work, the loop direction changes for an α_o greater than that for maximum steady lift. This difference may result from several sources. One of these is revealed by examination of the simplified model for $\Gamma(t)$ in equation (4), which is seen to be incapable of predicting a figure eight type hysteresis loop.

Notice in Figure 3 that the predicted hysteresis loops are closely aligned with the steady lift curve. This alignment, which is primarily determined by the value of Γ_{11}, seems adequate in each of the results. Of more interest perhaps is the behavior and influence of Γ_{10}. This parameter is largely responsible for the thickness of the hysteresis loops and it alone determines the direction in which they progress. Positive values of Γ_{10} produce clockwise directions, whereas negative values of Γ_{10} produce counterclockwise loops. In Figure 5 the effect of frequency, ω, on Γ_{10} is illustrated for three different problems. The present work is labeled "oscillating cylinder." The curve denoted by "oscillating stream" was obtained by applying the present analysis to the system in which the stream

is peridocally oscillating about a stationary elliptic cylinder. Just such a potential flow is obtained from equation (2) by omitting the Ω_z term. The last curve was obtained by casting the work of Moore[7] in the Γ_{10} notation. In his work, Moore also analyzed the case with the stream oscillating about the stationary elliptic cylinder. Judging from experimental airfoil results in which the hysteresis loops collapse at the large frequencies, if test data were available for an elliptic cylinder, the general slope of the Γ_{10} with ω curve would likely be the same as that shown, only shifted up into the quadrant where Γ_{10} is positive. Figure 5 also indicates that elimination of several simplifying assumptions made by Moore[7] in his earlier work signficantly affects the unsteady lift prediction.

In Figure 6 the movement of the separation points on both the upper and lower surfaces is depicted for $\alpha_o = 9^0$ as the angle-of-attack goes through one complete cycle. This movement is obtained from equations (13) and (24) using the values of C_1 and C_2 given in Table 2. In Figure 6 the effect of increasing the frequency is to produce a type of phase shift, best observed at $\omega t = \pi$, in the movement of the upper separation point. Notice that the lower separation points are practically stationary whereas in Figure 6 the upper separation point traverses a segment of the body surface equal to about 30 percent of the total chord. Also, the amplitude of the upper surface separation point movement is vastly different for each half cycle of the angle-of-attack variation. For example, with instantaneous $\alpha(t) = 9.5^0$, the forward movement of the separation point is approximately one half as great as the rearward movement observed when $\alpha(t) = 8.5^0$. For the $\omega = 0.10$ curve in Figure 6 a type of phase shift indicates that the separation point lies forward of that expected from steady results. Now applying the logic derived from steady boundary layer experience, the lift is expected to be less than the corresponding steady lift. That is the case as seen by examining Figure 3

for $\alpha_o = 9^0$. Thus the movement of the upper separation point in Figure 6 appears to be consistent with the predicted values of unsteady lift.

Perhaps the most interesting aspect of this analysis is a comparison presented in Figure 7 of the present results with the case where the stream is oscillating about a stationary elliptic cylinder. For values of α_o of approximately eight degrees or less, the predicted hysteresis loops for these two cases are very similar. However, at angles-of-attack in the stall region, Γ_{10} is positive for the oscillating elliptic cylinder (clockwise direction to the loop) in contrast to a negative value of Γ_{10} (counterclockwise loop) obtained when using the potential flow distribution for the stationary elliptic cylinder in an oscillating stream. This result seems to support the following hypothesis made by Moore[7]: "It may be that different directions of hysteresis should be expected when the airfoil oscillates and when, as in the present study, the stream direction oscillates." Indeed it appears that the clockwise direction of the hysteresis loop, which agrees with experimental airfoil results, is a direct consequence of including the Ω_z term in the expression for $u_\delta(x,t)$ which alters the form of $u_{\delta_{10}}$ to produce a positive value of Γ_{10}. Physically this additional term seems to describe the influence on the potential flow of the added mass effect associated with an accelerating body in unsteady motion. Thus, the experimentally observed phenomenon that the unsteady lift leads the periodic angle-of-attack change may be at least partially explained by including the Ω_z term in the potential flow description.

SUMMARY

An unsteady momentum integral technique has been employed to analyze the laminar, two-dimensional, unsteady boundary layer on an elliptic cylinder oscillating periodically in a steady freestream. The dynamic lift characteristics and the unsteady behavior of the boundary layer are predicted for several nominal angles-of-attack over a range of oscillation frequencies.

The basic approach was to represent the boundary layer parameters by a steady-state term plus an unsteady perturbation proportional to $\Delta\alpha$, to transform the usual boundary layer coordinate system such that the location of the separation points appear steady in the new coordinate system, and to relate the rate at which vorticity is shed into the wake to the time rate of change of circulation.

The predicted hysteresis loop direction was found to change from counterclockwise to clockwise as the mean angle-of-attack was increased from two degrees to within the stall region. This direction change was shown to compare favorably with experimental results for cylinders of airfoil cross section with the principal difference being that the experimental results indicate the direction change occurs at an angle-of-attack prior to that for maximum steady lift, whereas the present study predicts a direction change at some mean angle-of-attack after maximum steady lift. Probably the most significant finding resulted from a comparison of the hysteresis loop predicted at a high angle-of-attack using the potential flow for an oscillating body in a stationary stream to the loop obtained using the same solution techniques, only changing the potential flow to describe a system in which the body is stationary but the stream oscillates. In each case the hysteresis loops were similar in structure but with opposite directions. The clockwise direction of

the predicted loop using the potential flow for the oscillating body agrees with experimental observations, in contrast to the counterclockwise direction obtained for the system with the body stationary. The potential flows for the two systems differ only by a term proportional to $\dot{\alpha}(t)$ which describes the influence on the potential flow of the added mass effect normally observed when a body is accelerating in unsteady flow.

An obvious shortcoming in the present model is the assumption of laminar flow, particularly on the upper surface of the elliptic cylinder. By considering the laminar separation point as the point of wake onset, an excessively large portion of the body surface is exposed to the wake flow, whose effect on the potential flow was assumed negligible. A logical extension of the present work and one which is being undertaken now, is to include an unsteady turbulent boundary layer model.

REFERENCES

1. Halfman, R. C., H. C. Johnson, and S. M. Haley. "Evaluation of High-Angle-of-Attack Aerodynamic-Derivative Data and Stall-Flutter Prediction Techniques." NACA TN 2533, 1951.

2. Liiva, Jaan, F. J. Davenport, Lewis Gray, and I. C. Walton. "Two-Dimensional Tests of Airfoils Oscillating Near Stall-Volume 1, Summary and Evaluation of Results." USAAVLABS Tech. Report 68-13A, U. S. Army Aviation Material Laboratories, Fort Eustis, Virginia, 1968.

3. Ham, N. D. "Aerodynamic Loading of a Two-Dimensional Airfoil During Dynamic Stall." AIAA J. Vol. 6, No. 10, October 1968, pp 1927-1934.

4. Ericsson, L. E. and J. P. Reding. "Dynamic Stall of Helicopter Blades." Paper Presented at the 26th Annual National Forum of the American Helicopter Society, Washington, D. C., 1970.

5. Crimi, Peter. "Dynamic Stall." AGARD Report-AG-172, 1973.

6. Patay, S. A., "Leading Edge Separation on an Airfoil During Dynamic Stall." ASRL TR 156-1, MIT Aeroelastic and Structures Research Laboratory, Cambridge, Massachusetts, 1969.

7. Moore, F. K. "Lift Hysteresis at Stall as an Unsteady Boundary-Layer Phenomenon." NACA TN 3571,

8. Sears, W. R. "Some Recent Developments in Airfoil Theory." J. Aeronautical Sciences, Vol. 23, No. 5, May 1956, pp. 490-499.

9. Kochin, N. E., I. A. Kibel, and N. V. Roze. "Theoretical Hydromechanics," John Wiley and Sons, Inc., New York, New York, 1964, pp. 320-332.

10. Moore, F. K. "On the Separation of the Unsteady Laminar Boundary Layer." Boundary Layer Research, Springer-Verlog, Berlin, 1958, p. 296-310.

11. Rott, N. "Unsteady Flow in the Vicinity of a Stagnation Point." Quarterly Applied Mathematics, Vol. 13, 1956, pp. 444-451.

12. Teipel, Ingolf. "Calculation of Unsteady Laminar Boundary Layers by an Integral Method." Z. Flugwiss, Vol. 18, 1970, pp. 58-65.

13. Dryden, H. L. "Computation of the Two-Dimensional Flow in a Laminar Boundary Layer." NACA TR 497, 1934.

14. Howarth, L. "The Theoretical Determination of the Lift Coefficient for a Thin Elliptic Cylinder. Proceedings of Royal Society (London) A, Vol. 149, 1935, pp. 558-586.

15. Taylor, G. I. "Note on the Connection Between the Lift on an Airfoil in a Wind and the Circulation Round It. Philosophical Transactions A, Vol. 225, 125, pp. 238-245.

NOMENCLATURE

a	major axis of ellipse
b	minor axis of ellipse
b_1, b_2	arbitrary constants chosen to model the velocity profile
C_1, C_2	scaling constants in the function q(t)
C_ℓ	two-dimensional lift coefficient
$C_{\ell_{max}}$	maximum two-dimensional lift coefficient
L	length of semi-chord (ft)
$q(t)$	function of time used to scale the streamwise coordinate
$q_1(t)$	function equal $C_1 \cos \omega t + C_2 \sin \omega t$
r	y/δ
T_1, T_2	test functions used in describing the unsteady circulation criterion
t	non-dimensional time
U	freestream velocity (ft/sec)
u	non-dimensional boundary layer velocity in the x-direction
u_δ'	potential flow velocity (ft/sec)
u_{δ_0}	steady component of the potential flow
$u_{\delta_{10}}$, $u_{\delta_{11}}$	unsteady components of the potential flow
v	non-dimensional boundary layer velocity in the y-direction
w	complex velocity potential
X'	coordinate axis coinciding with major axis of ellipse
x	non-dimensional boundary layer coordinate along the body surface
x_s	x-coordinate at separation
Y'	coordinate axis coinciding with minor axis of ellipse
y	non-dimensional boundary layer coordinate normal to the body surface
Z	δ_0^2

α	angle-of-attack
α_o	mean angle-of-attack
β	fineness ratio of the elliptic cylinder
Γ'	unsteady circulation (ft^2/sec)
Γ_o	steady component of the circulation
Γ_{10}, Γ_{11}	unsteady components of the circulation
$\Delta\alpha$	increment of angle-of-attack
δ	boundary layer thickness
${}^1\delta_{10}$, ${}^2\delta_{10}$ ${}^3\delta_{10}$, ${}^1\delta_{11}$ ${}^2\delta_{11}$, ${}^3\delta_{11}$	form the boundary layer thickness components δ_{10} and δ_{11}
δ^*	displacement thickness
θ	momentum thickness
λ	boundary layer shape factor
ξ	transformed streamwise coordinate
ξ_s	location of separation in the ξ coordinates
τ_w	wall shear
Ω_z'	angular velocity (rad/sec)
ω	non-dimensional oscillation frequency
$(\dot{})$	time derivative
$(\bar{})$	overbars denote quantities at the upper separation point
$(\underline{})$	underbars denote quanties at the lower separation point
Subscripts:	
0	steady components
10,	unsteady components multiplying $\Delta\alpha \cos \omega t$
11,	unsteady components multiplying $\Delta\alpha \sin \omega t$

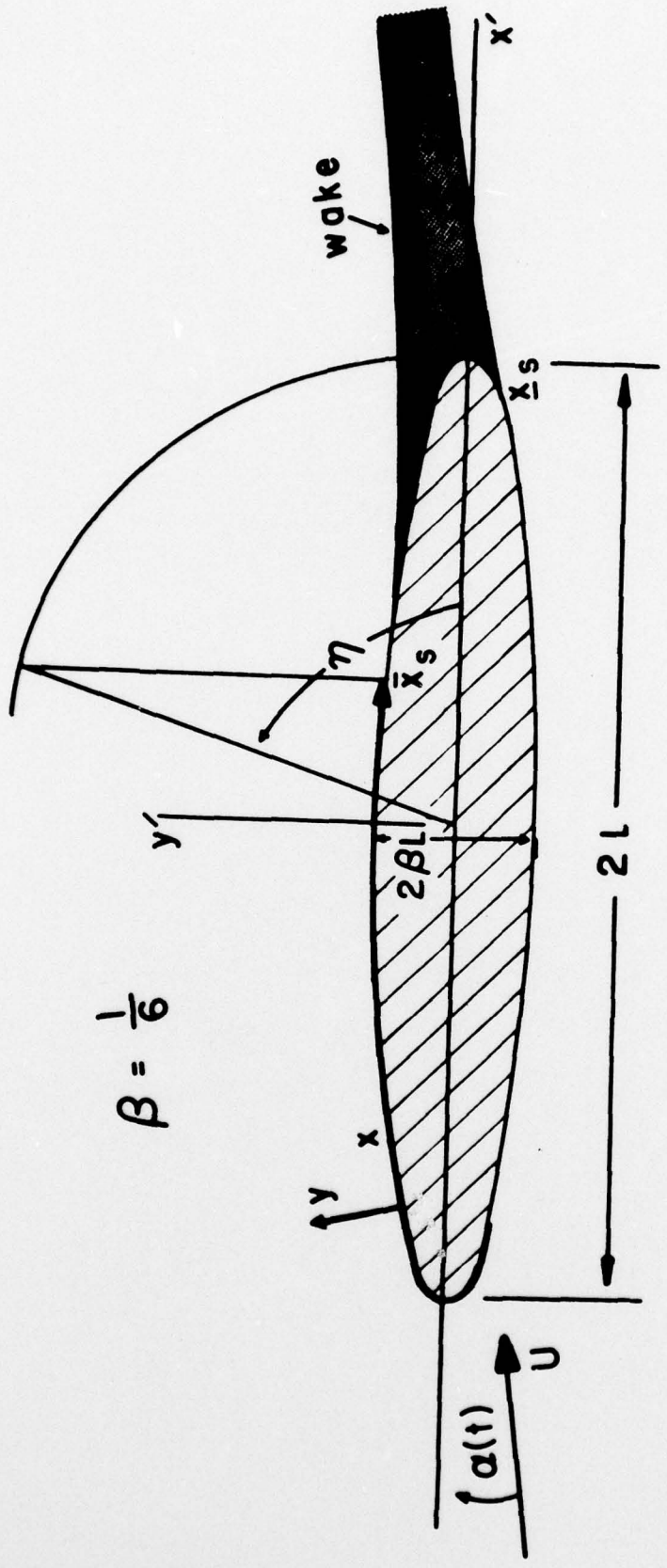

Figure 1. Basic coordinate system and body orientation

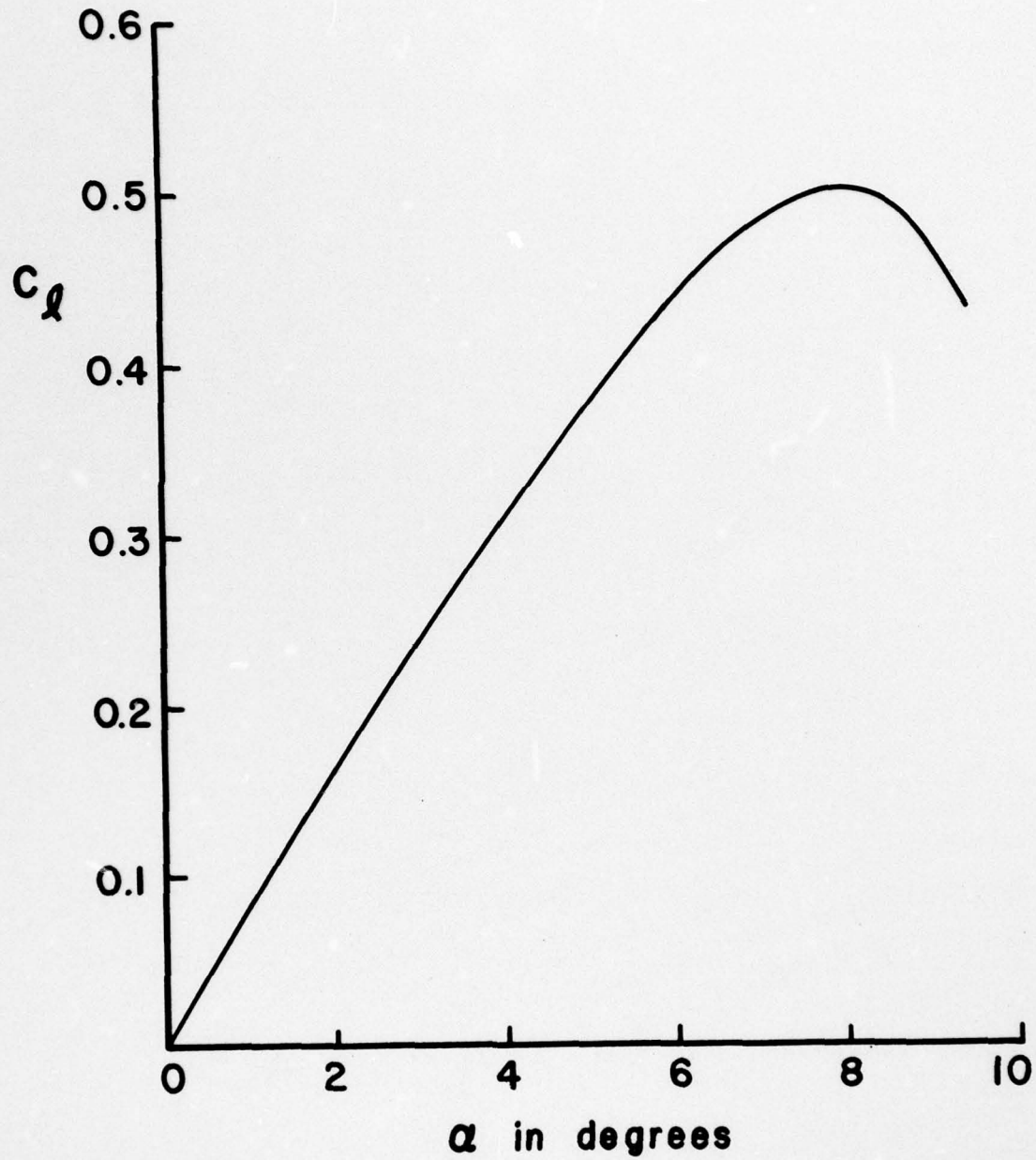

Figure 2. Steady-state lift curve for the elliptic cylinder

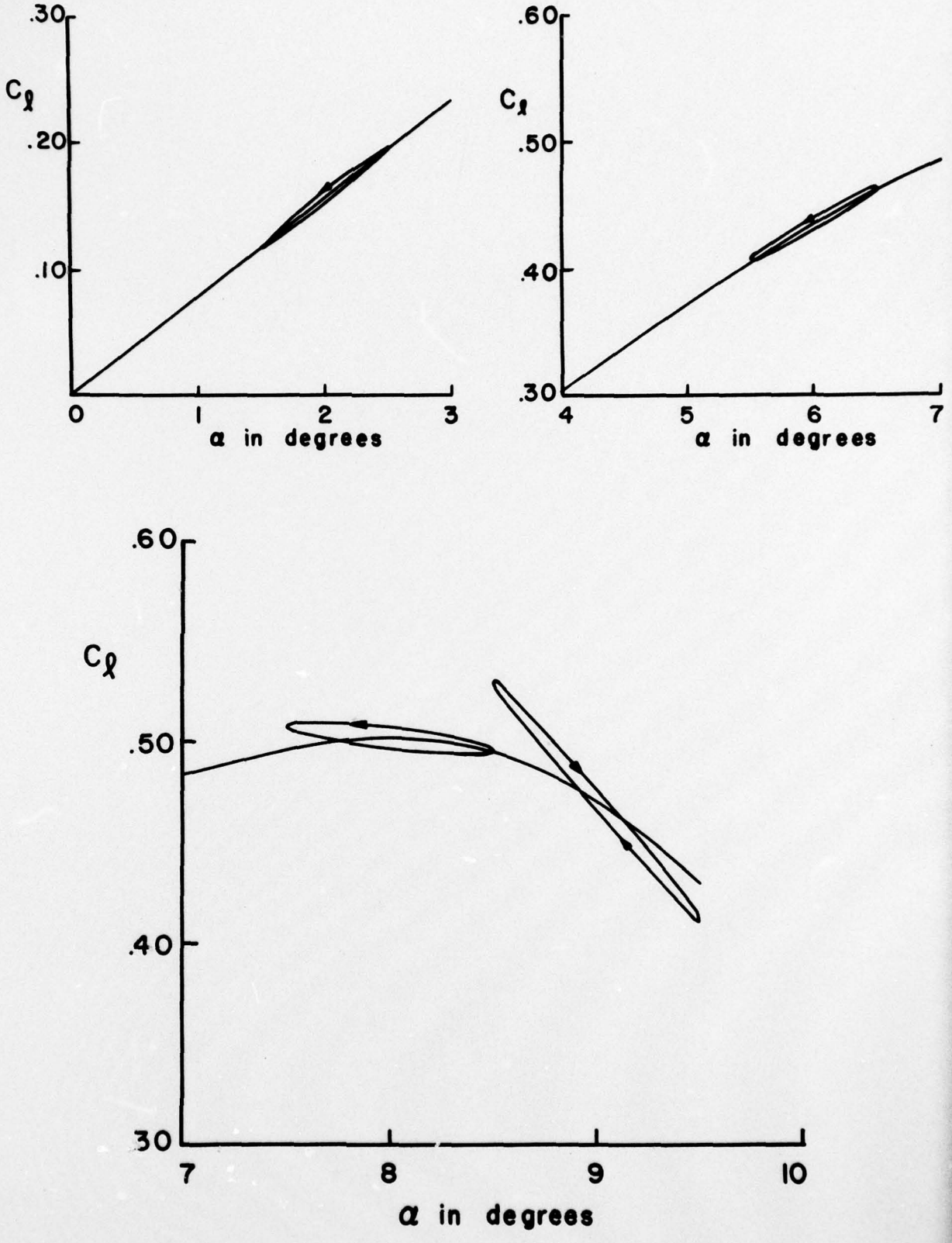

Figure 3. Unsteady lift hysteresis for several values of α_o with $\omega = 0.10$

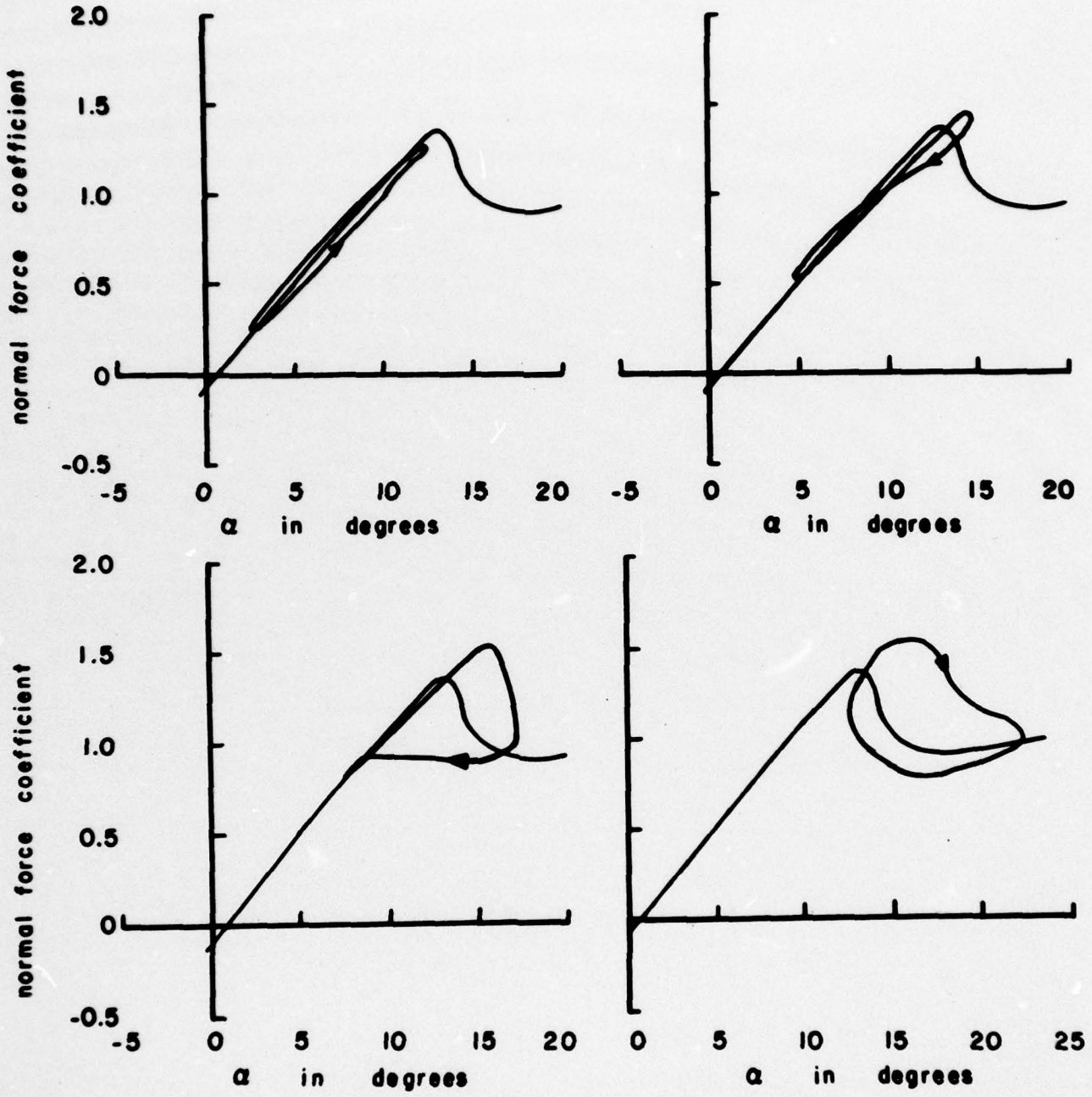

Figure 4. Unsteady lift hysteresis for a Vertol 23010-1.58 airfoil at constant oscillation frequency (Ref. 2)

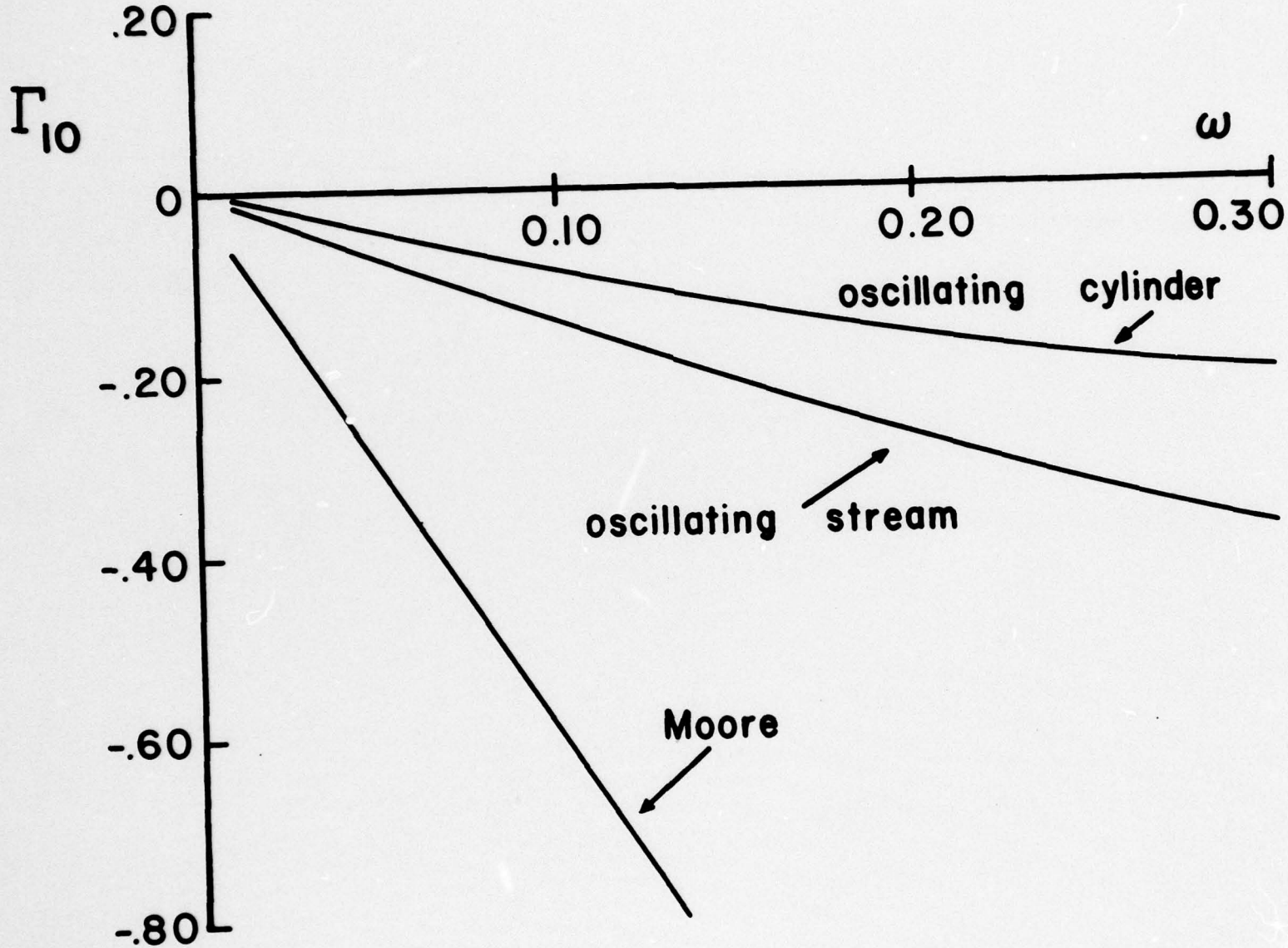

Figure 5. Variation of Γ_{10} with frequency at $\alpha_o = 8^0$

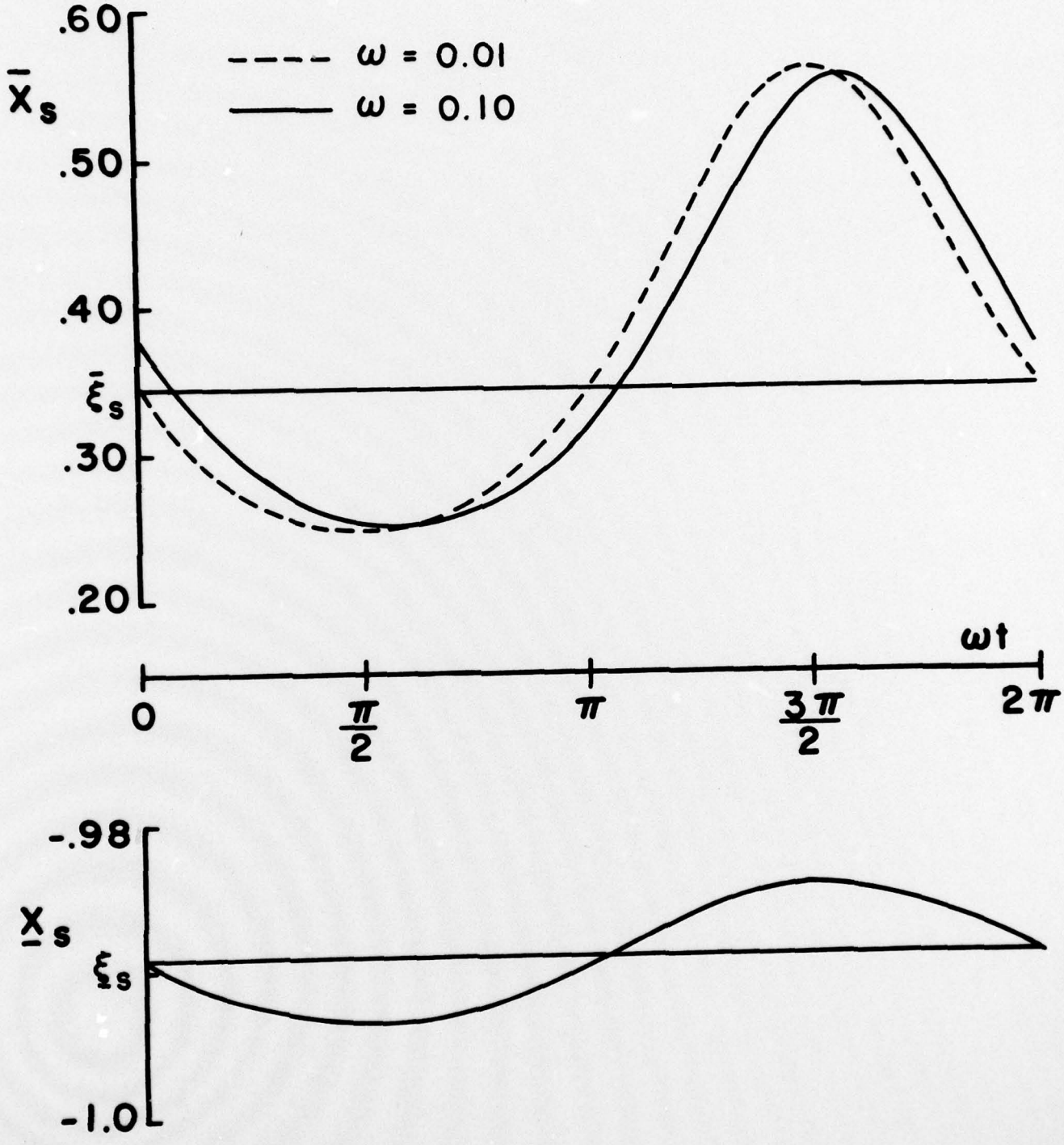

Figure 6. Movement of the upper and lower surface separation points for $\alpha_o = 9^0$

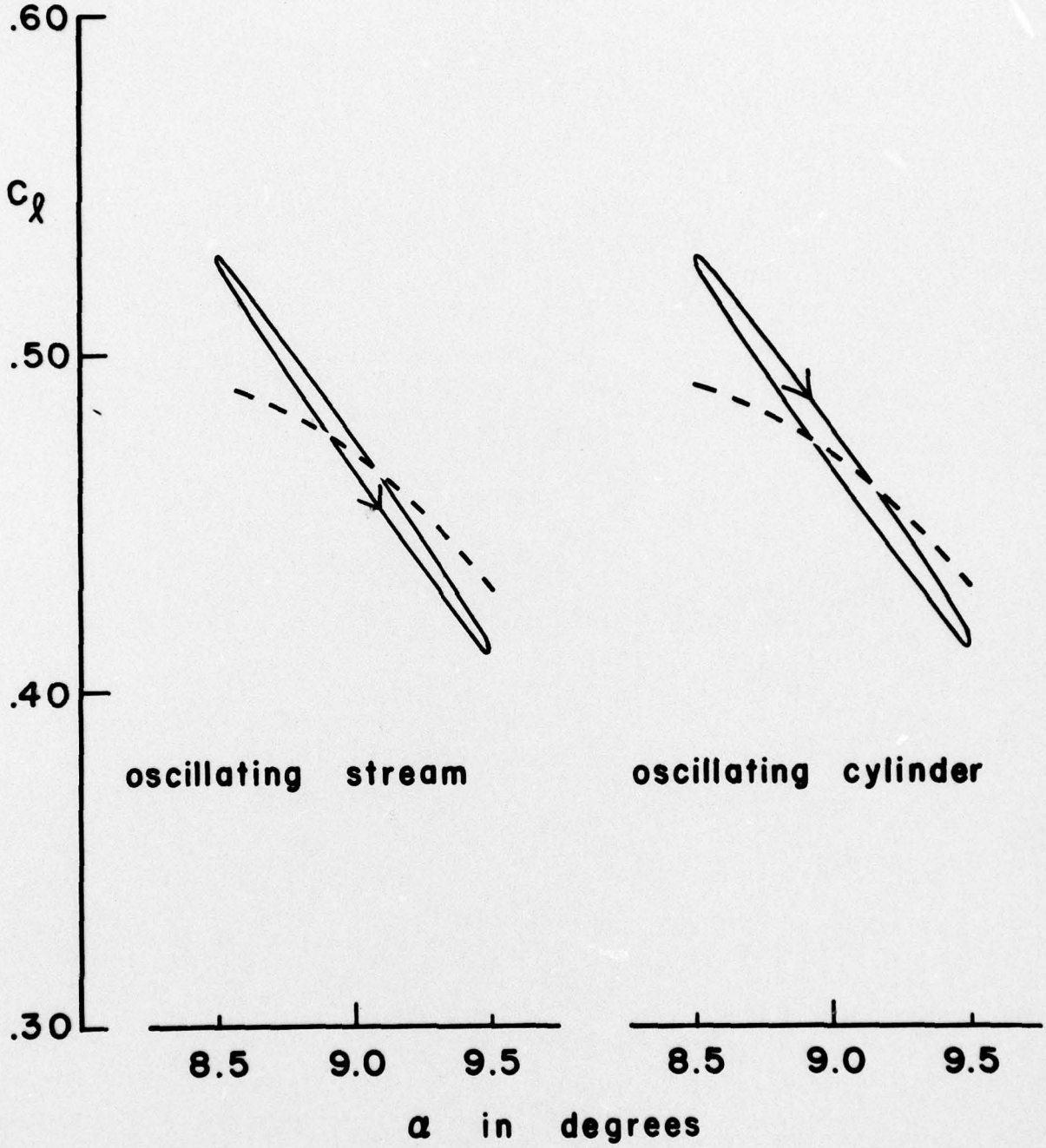

Figure 7. Contrasting hysteresis loop directions for $\omega = 0.10$